Ab Initio Calculation of Photoionization and Inelastic Photon Scattering Spectra of He below the $N = 2$ Threshold in a dc Electric Field

Andrej Mihelič* and Matjaž Žitnik
Jožef Stefan Institute, Jamova 39, 1000 Ljubljana, Slovenia
(Received 14 November 2006; published 15 June 2007)

We study the Stark effect on doubly excited states of the helium atom below $N = 2$. We present the *ab initio* photoionization and total inelastic photon scattering cross sections calculated with the method of complex scaling for field strengths $F \leq 100$ kV/cm. The calculations are compared to the measurements of the ion [Phys. Rev. Lett. **90**, 133002 (2003)] and vacuum ultraviolet fluorescence yields [Phys. Rev. Lett. **96**, 093001 (2006)]. For the case of photoionization and for incident photons with polarization vector **P** parallel to the electric field **F**, we confirm the propensity rule proposed by Tong and Lin [Phys. Rev. Lett. **92**, 223003 (2004)]. Furthermore, the rule is also shown to apply for $\mathbf{F} \perp \mathbf{P}$ and for the case of the inelastic scattering in both experimental geometries.

DOI: 10.1103/PhysRevLett.98.243002 PACS numbers: 32.60.+i, 31.25.Jf, 32.70.Cs, 32.80.Fb

The helium atom is considered a standard atomic system for studying electron correlation [1], since it is relatively easy to manipulate experimentally while still remaining computationally manageable. Doubly excited helium has been investigated extensively since the first photoabsorption measurements of Madden and Codling [2], both theoretically (Ref. [3], and references therein) and experimentally (cf. [4,5]). Helium doubly excited states are affected by collective electron dynamics reaching beyond the standard mean field approximations. Their energies, lifetimes, and oscillator strengths are of interest in plasma physics and astrophysics (e.g., [6]). For a long time, autoionization has been deemed to be the only non-negligible decay channel of doubly excited states, whereas the fluorescence decay has been completely disregarded. Only the recent experiments demonstrated the importance of radiative decay of doubly excited states [7–9].

Apart from the dipole allowed $^1P^o$ states, there are many others that remain inaccessible from the ground state with simple photoexcitation. If the atom is subject to an external electric field, these *dark states* can be accessed indirectly via the Stark-induced coupling with the $^1P^o$ states. Detailed studies of the Stark effect on doubly excited states are just beginning. Harries *et al.* [10] measured the photoionization (PI) cross sections in strong dc electric fields $\mathbf{F} \parallel \mathbf{P}$ with strengths up to 84.4 kV/cm in the region of the $6a$—$8a$ $^1P^o$ resonances below $N = 2$. The experiment confirmed the theoretical predictions of Chung, Fang, and Ho [11], who estimated that field strengths of the order of 50 kV/cm are required in the $n = 6$ region for measurable electric field effects. Tong and Lin [12] proposed the propensity rule to describe the groups of doubly excited states that are preferentially populated in the ground state photoexcitation. Furthermore, it was shown theoretically that, in the energy region of low lying resonances, the spin-orbit interaction negligibly interferes with the Stark effect [13]. On the other hand, several experimental groups recently measured the Stark effect on the fluorescence yield (FY) of doubly excited states [14–17]. In contrast with the PI signal, it was shown that even field strengths of only a few kV/cm can substantially change the spectra below $N = 2$.

For detailed analysis of spectral features induced by external electric fields, a detailed theoretical modeling is essential. We present the first *ab initio* calculations of the PI cross sections that explain the measured signal [10] for the parallel experimental geometry $\mathbf{F} \parallel \mathbf{P}$ and give the first predictions for $\mathbf{F} \perp \mathbf{P}$. Furthermore, the total inelastic photon scattering cross sections in strong fields are calculated for the first time for both geometries. The spectra are also compared to the weak electric field experimental data [15]. The present calculations supersede our first-order perturbation calculations for field strengths below 5 kV/cm and the $n \leq 10$ manifold of states [18].

The method of complex scaling [19,20] was used to calculate the cross sections. It allows an exact representation of the atomic continuum using an $\mathcal{L}^2$ basis set: Complex scaled wave functions of autoionizing states obtained by diagonalization of the complex scaled Hamilton operator are square integrable. Approaches similar to those dealing with bound states are thus employed to calculate physical parameters associated with the resonance states. The eigenstates of the complex scaled nonrelativistic Hamilton operator, which describes the helium atom in an electric field, were expanded in the basis of field free eigenstates with the total angular momenta $L \leq 10$ of even and odd parity. The field free eigenstates were obtained by a configuration interaction expansion in a Sturmian basis employing several different pairs of radial scaling parameters of the two electrons [21]. In this way we were able to accurately calculate *asymmetrically excited* states with $n \leq 15$, where on average one of the electrons moves at large radial distances, while the other remains close to the nucleus. The basis for the selected $^1L^\pi$ symmetry typically consisted of about 10^4 Sturmian functions and allowed all of the states to be obtained within a single diagonalization. The errors of the calculated zero field

 © 2007 The American Physical Society

energies and autoionization widths range from 10^{-5} a.u. for $n = 2, 3$ $^1S^e$, $^1P^o$, $^1D^e$, and $^1F^o$ doubly excited states and decrease to 10^{-9} a.u. and less for higher lying states [22]. The high energy cut for the field free eigenstates was set below the $N = 3$ threshold to account unambiguously for all of the eigenstates converging to $N = 1, 2$ and resulted in the total Hamilton matrix with dimensions 2557×2557.

To calculate the ground state PI cross sections, the familiar resonance cross section expression [20] was modified to account for the radiative decay of the resonance states [22]:

$$\sigma_n = 4\pi\alpha\omega_0 \mathrm{Im} \frac{\langle\overline{\Psi_{n\theta}}|D_\theta^0|\Psi_{g\theta}\rangle^2 - b_n|\langle\overline{\Psi_{n\theta}}|D_\theta^0|\Psi_{g\theta}\rangle|^2}{E_n - E_g - \omega_0 - i(\Gamma_n^a + \Gamma_n^r)/2}, \quad (1)$$

where $|\Psi_{g\theta}\rangle$ and $|\Psi_{n\theta}\rangle$ are the complex scaled ground and resonance state kets, respectively, ω_0 is the incident photon energy, and $D_\theta^0 = e^{i\theta}\hat{\mathbf{e}}_0 \cdot (\mathbf{r}_1 + \mathbf{r}_2)$ is the complex scaled dipole operator, where θ is the "rotation angle", $\mathbf{r}_1$ and $\mathbf{r}_2$ the positions of the two electrons, and $\hat{\mathbf{e}}_0$ the polarization vector of the incident photons. The autoionization and fluorescence decay widths of the resonance are denoted by Γ_n^a and Γ_n^r, respectively, whereas $b_n = \Gamma_n^r/(\Gamma_n^a + \Gamma_n^r)$ is the fluorescence branching ratio. The notation $\langle\overline{\cdots}|$ means that the deconjugated radial part of the wave function is to be used in the calculation of the radial integrals. Equation (1) results in an expression similar to the one derived by Robicheaux *et al.* [23]. While the autoionization widths and the resonance energies are given by the eigenvalues $E_n - i\Gamma_n^a/2$ of the complex scaled Hamiltonian, the radiative widths were calculated from the real parts of the squared matrix elements between the complex scaled states:

$$\Gamma_n^r = \frac{\alpha^3}{2\pi} \sum_{m,\beta} \int d\Omega (E_n - E_m)^3 \mathrm{Re}\langle\overline{\Psi_{m\theta}}|D_\theta^\beta|\Psi_{n\theta}\rangle^2. \quad (2)$$

The summation runs over final singly excited states and both perpendicular polarizations $\hat{\mathbf{e}}_\beta$ of the emitted photon, and the integration is over the photon solid angle. In fact, Γ_n^r is proportional to the *integrated* resonance cross section [3]. It may be seen that the latter—neglecting the energy dependence of Γ_n^a in the region of the resonance—is equivalent to treating the resonance state as a purely bound state [24]. For $F \leq 100$ kV/cm, the calculated autoionization widths of the final singly excited states remain 2–3 orders of magnitude below the total widths of the doubly excited states from which they are most probably populated. Similarly, according to our multiconfiguration Hartree-Fock calculations, the dipole transition probabilities to lower lying doubly excited states are at most of the order of 10^{-10} a.u. and have been neglected. It is then a fair approximation to include only the singly excited final states in Eq. (2) and to treat these states as bound.

The energies and widths of the doubly excited states in the $n = 6$ energy region are listed in Table I. The labeling

TABLE I. Energies, autoionization, and fluorescence widths (in atomic units) for the $n = 6$ energy region of the doubly excited singlet states for $F = 0$ and $F = 84.4$ kV/cm $\approx 1.64 \times 10^{-5}$ a.u. The quantization axis points along the electric field vector $\mathbf{F}$. Numbers in parentheses indicate powers of ten. Autoionization widths that are too small to be reliably calculated are omitted ($\cdots$). For the nonzero field, the weights w (square modulus, in %) of the leading field free components (l.c.) are given.

	$F = 0$			$F = 84.4$ kV/cm, $M = 0$					$F = 84.4$ kV/cm, $\lvert M\rvert = 1$				
State	$-E$	Γ^a	Γ^r	l.c.	$-E$	Γ^a	Γ^r	w	l.c.	$-E$	Γ^a	Γ^r	w
$6b\ P^o$	0.517 936 917	5.30(−7)	2.03(−7)	$6b\ P^o$	0.518 215 592	2.32(−5)	1.72(−7)	62	$5c\ P^o$	0.518 110 400	4.75(−7)	7.51(−8)	91
$6a\ S^e$	0.517 640 889	1.14(−4)	1.43(−7)	$6a\ S^e$	0.517 409 314	7.16(−5)	1.64(−7)	69	$6b\ P^o$	0.517 939 953	1.29(−6)	2.16(−7)	93
$6a\ P^e$	0.516 208 609	0	2.37(−7)	$6a\ P^e$	0.516 288 425	$\cdots$	2.30(−7)	94	$6a\ P^e$	0.516 317 791	2.07(−6)	2.27(−7)	91
$6b\ D^e$	0.515 453 312	6.60(−5)	1.47(−7)	$6b\ D^e$	0.515 551 667	5.71(−5)	1.49(−7)	88	$6b\ D^e$	0.515 548 907	5.79(−5)	1.49(−7)	89
$6a\ D^o$	0.514 833 587	0	2.39(−7)	$6a\ D^o$	0.514 946 653	$\cdots$	2.37(−7)	72	$6a\ D^o$	0.514 952 605	1.55(−6)	2.35(−7)	74
$6a\ P^o$	0.514 733 425	3.80(−5)	1.88(−7)	$6a\ P^o$	0.514 925 667	2.84(−5)	1.60(−7)	74	$6a\ P^o$	0.514 832 592	2.49(−5)	1.68(−7)	69
$6b\ G^e$	0.514 226 769	6.8(−8)	2.23(−7)	$6b\ G^e$	0.514 681 373	3.44(−6)	2.28(−7)	48	$6b\ G^e$	0.514 669 793	3.68(−6)	2.28(−7)	48
$6b\ F^o$	0.514 166 715	2.48(−6)	2.14(−7)	$6a\ F^o$	0.514 410 254	5.09(−6)	5.35(−8)	37	$6a\ F^o$	0.514 395 898	4.76(−6)	5.66(−8)	37
$6a\ F^e$	0.514 113 204	0	2.42(−7)	$6a\ G^o$	0.514 347 239	$\cdots$	2.41(−7)	49	$6a\ G^o$	0.514 346 678	2.0(−8)	2.38(−7)	47
$6b\ H^o$	0.514 086 145	6(−10)	2.32(−7)	$6b\ I^e$	0.514 274 140	1.85(−6)	2.07(−7)	33	$6b\ I^e$	0.514 271 988	1.73(−6)	2.08(−7)	32
$6b\ I^e$	0.514 022 568	$\cdots$	2.36(−7)	$6a\ H^o$	0.514 045 800	3.65(−6)	9.68(−8)	35	$6a\ H^o$	0.514 044 887	3.40(−6)	9.75(−8)	34
$6a\ G^o$	0.513 982 234	0	2.42(−7)	$6c\ F^o$	0.513 974 406	8.0(−8)	2.24(−7)	44	$6a\ H^e$	0.513 975 469	2.13(−7)	2.35(−7)	47
$6a\ F^o$	0.513 962 516	3(−9)	4.31(−8)	$6a\ H^e$	0.513 959 689	$\cdots$	2.42(−7)	59	$6c\ F^o$	0.513 945 366	3.80(−7)	2.25(−7)	37
$6a\ D^e$	0.513 951 996	3.85(−6)	1.20(−7)	$6b\ I^e$	0.513 933 919	2.14(−6)	1.65(−7)	33	$6b\ F^o$	0.513 932 937	1.48(−6)	1.70(−7)	21
$6a\ H^e$	0.513 936 261	0	2.43(−7)	$6a\ H^o$	0.513 716 596	2.68(−6)	1.24(−7)	26	$6a\ D^e$	0.513 724 851	2.51(−6)	1.27(−7)	26
$6a\ G^e$	0.513 909 579	1(−10)	2.88(−8)	$6b\ G^e$	0.513 639 823	1.13(−6)	1.78(−7)	22	$6b\ G^e$	0.513 658 144	1.65(−6)	1.81(−7)	24
$6a\ H^o$	0.513 895 815	$\cdots$	1.79(−8)	$6c\ G^e$	0.513 627 437	1.58(−6)	2.04(−7)	36	$6a\ G^o$	0.513 602 356	3.92(−7)	2.23(−7)	33
$6c\ G^e$	0.513 664 386	$\cdots$	2.32(−7)	$6a\ G^o$	0.513 591 944	$\cdots$	2.42(−7)	48	$6c\ G^e$	0.513 583 389	2.01(−7)	2.22(−7)	43
$6c\ F^o$	0.513 543 372	$\cdots$	2.26(−7)	$6a\ F^o$	0.513 407 736	2.18(−6)	8.62(−8)	35	$6a\ F^o$	0.513 426 252	1.45(−6)	8.93(−8)	36
$6c\ D^e$	0.513 311 130	8(−9)	2.15(−7)	$6c\ F^o$	0.513 305 573	2.11(−6)	1.87(−7)	32	$6c\ F^o$	0.513 180 282	3.26(−7)	2.12(−7)	42
$6c\ P^o$	0.512 790 392	$\cdots$	7.61(−8)	$6c\ D^e$	0.512 957 142	8.92(−7)	1.94(−7)	41	$7b\ P^o$	0.512 835 080	3.68(−6)	9.46(−8)	45
$6b\ S^e$	0.512 762 516	2.00(−5)	8.55(−8)	$6c\ P^o$	0.512 274 095	3.48(−5)	5.09(−8)	41	$7b\ P^o$	0.512 594 400	8.36(−7)	2.05(−7)	43

of Tong and Lin [12] is used to group doubly excited states with similar asymptotic correlation properties. This differs from the simple classification scheme introduced by Lipsky [25] (and used in Ref. [10]). The calculated PI cross sections in the $6a$ and $7a$ $^1P^o$ energy region (65.008 and 65.117 eV, respectively) are shown in Fig. 1. The agreement with the experimental spectra for $\mathbf{F} \parallel \mathbf{P}$ is generally good, especially for higher field strengths [Fig. 1(b)]. At lower fields, large scale oscillations are present. Since the theory completely describes spectral features at high electric fields, these oscillations are believed to be of nonatomic origin. The zero field ordering of the states matches the already reported one [12], with the exception of the a group of states. For $n = 6$, the following states appear in order of increasing energy: $^1S^e$, $^1P^o$, $^1F^o$, $^1D^e$, $^1G^e$, and $^1H^o$. In the $n = 7$ energy region, the $7a$ $^1I^e$ state is appended to the sequence. The inclusion of high orbital momenta with $L \lesssim n$ is seen to be essential for the calculation even in the case of moderate principal quantum numbers: The peaks following the $6a$ and $7a$ $^1P^o$ resonances cannot be reproduced otherwise. The small peaks

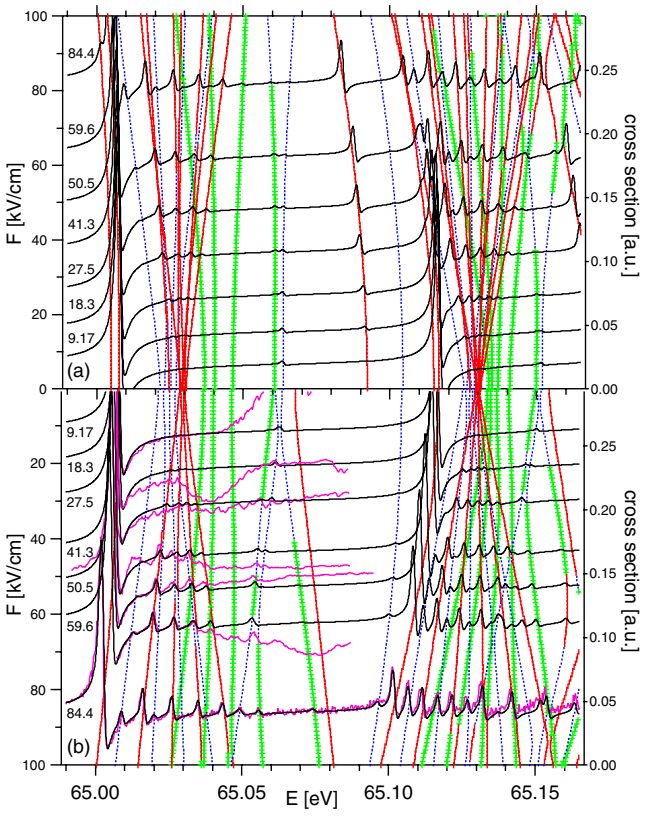

FIG. 1 (color online). (a) The calculated photoionization for $\mathbf{F} \perp \mathbf{P}$. (b) The calculated (black) and the measured [10] photoionization for $\mathbf{F} \parallel \mathbf{P}$. The spectra are shifted vertically so that their baselines correspond to the applied field strength (left axis). In the underlying Stark maps, a solid red line, a dotted blue line, and green plus signs are used for the leading components of the a, b, and c groups, respectively. The measured data are scaled to match the theory, which is broadened with a 1.4 meV FWHM Gaussian.

preceding the $6a$ (not shown in Fig. 1) and $7a$ $^1P^o$ resonances may be attributed to the states with the nb $^1D^e$ ($n = 6, 7$) leading components. This differs from the $^1D^o$ designation suggested in Ref. [10] but is in accord with Ref. [12]. The perpendicular geometry $\mathbf{F} \perp \mathbf{P}$ also allows the excitation of the states with parity $(-1)^{L+1}$. Several additional states are therefore induced by the field, most strongly the na $^1P^e$ states, but also the na $^1D^o$ states are expected to be visible at high field strengths. Note that the $^1S^e$ states are not accessible in this geometry.

The majority of prominent peaks in the PI spectrum belong to the a group because the oscillator strength of the dark a states stems predominantly from the strong field-induced coupling with the optically allowed a $^1P^o$ states, which bear most of the field free oscillator strength. This is in accord with the propensity rule [12]: The external electric field strongly couples states with similar correlation character. The rule seems to hold even better for $\mathbf{F} \perp \mathbf{P}$ [Fig. 1(a)], where the amplitudes of the b and c peaks remain below one-half of the a peak amplitudes.

The inelastic photon scattering cross section expression

$$\alpha^4 \omega_0 \sum_{m,\beta} \omega_{mg}^3 \int d\Omega \left| \sum_n \frac{\langle \overline{\Psi_{m\theta}} | D_\theta^\beta | \Psi_{n\theta} \rangle \langle \overline{\Psi_{n\theta}} | D_\theta^0 | \Psi_{g\theta} \rangle}{E_g + \omega_0 - E_n + i(\Gamma_n^a + \Gamma_n^r)/2} \right|^2 \tag{3}$$

($\omega_{mg} = E_g + \omega_0 - E_m$) was derived from the time-independent second-order perturbation theory, where the Green operator of the inelastic scattering term was expressed with the complex scaled Green operator. Elastic scattering contributions to the cross section were neglected, since they are several orders of magnitude below the contribution of the resonant term in the energy region of interest [22]. The calculated FY spectra for the perpendicular and parallel geometries are shown in Fig. 2. It is seen that the field strongly affects the cross section already at low field strengths. Again, the contributions from several additional field free states with parity $(-1)^{L+1}$ are present for $\mathbf{F} \perp \mathbf{P}$. For example, intense peaks may be seen to evolve from the zero field $^1P^e$ and $^1D^o$ states [Fig. 2(a)]. For $\mathbf{F} \parallel \mathbf{P}$, the intensities of the nc, $(n+1)b$ $^1P^o$ doublets rapidly decrease with the field strength. This occurs due to the presence of strongly autoionizing $^1S^e$ and $^1D^e$ states in the vicinity of the doublet. The field-induced coupling of the doublet results in a substantial increase of the autoionization width, so that the fluorescence branching ratio is drastically reduced, and the FY intensity decreases. The effect is weaker for $\mathbf{F} \perp \mathbf{P}$, where the Stark-induced coupling to the close lying $^1S^e$ states is zero. As in the case of PI, the intense peaks in the FY belong mostly to the a group. Several prominent peaks also occur that are attributed the b and c character, e.g., the nc, $(n+1)b$ $^1P^o$ doublets. Note that this does not contradict the propensity rule. Although the b and c $^1P^o$ states are excited with lower probability, they decay predominantly by fluorescence. Nevertheless, when the field is increased, the intensities

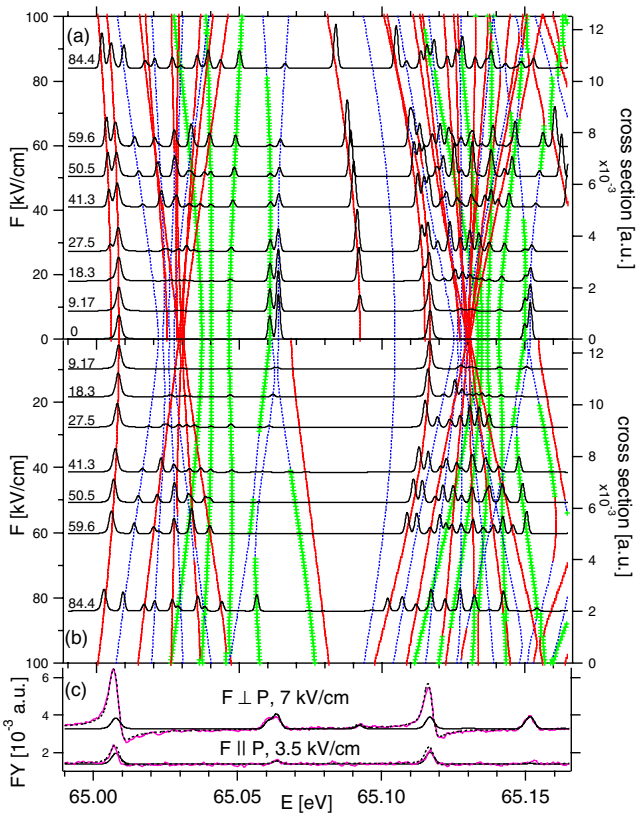

FIG. 2 (color online). As in Fig. 1 but for the inelastic photon scattering cross sections: (a) $\mathbf{F} \perp \mathbf{P}$ and (b) $\mathbf{F} \parallel \mathbf{P}$. (c) Comparison of the calculated cross sections (black curve), weighted sum (dashed curve, see text), and measured VUV FY spectra [15]. The theory is broadened with a 3.0 meV FWHM Gaussian.

of the a peaks are increased, while the b and c peaks generally decrease.

No measurements of the fluorescence yield of doubly excited helium are available for high field strengths. In Fig. 2(c), we compare the calculated primary FY spectra to the weak field vacuum ultraviolet (VUV) photon yield measurements of Prince *et al.* [15]. Since the majority of fluorescing atoms end in the ground state [26], the VUV yield is approximately proportional to the primary FY. The theory and experiment agree quite well, provided that an admixture of the (calculated) PI signal is added to the calculated FY. This additional spurious signal is strongest for the $a\,^1P^o$ resonances and high electric fields and is most probably due to the fluorescence generated by collisions of charged particles with the experimental equipment.

In conclusion, we have calculated the photoionization and inelastic photon scattering cross sections of doubly excited helium in a static electric field. The theory is in good agreement with the published experimental data and predicts the outcome in cases where the measurements are not available. It has been demonstrated that the propensity rule originates in the strong ground state dipole coupling to the a correlation group of doubly excited states and is manifested in both decay channels: autoionization and fluorescence.

We thank Gérard Lagmago Kamta for his kind advice on the calculations. We gratefully acknowledge the financial support from the Slovenian Ministry of Higher Education, Science, and Technology (research Program No. P1–0112).

*andrej.mihelic@ijs.si

[1] G. Tanner, K. Richter, and J.-M. Rost, Rev. Mod. Phys. **72**, 497 (2000).
[2] R. P. Madden and K. Codling, Phys. Rev. Lett. **10**, 516 (1963).
[3] J.-M. Rost *et al.*, J. Phys. B **30**, 4663 (1997).
[4] M. Domke, G. Remmers, and G. Kaindl, Phys. Rev. Lett. **69**, 1171 (1992).
[5] K. Schulz *et al.*, Phys. Rev. Lett. **77**, 3086 (1996).
[6] O. Marchuk *et al.*, J. Phys. B **37**, 1951 (2004).
[7] M. K. Odling-Smee *et al.*, Phys. Rev. Lett. **84**, 2598 (2000).
[8] J. E. Rubensson *et al.*, Phys. Rev. Lett. **83**, 947 (1999).
[9] F. Penent *et al.*, Phys. Rev. Lett. **86**, 2758 (2001).
[10] J. R. Harries *et al.*, Phys. Rev. Lett. **90**, 133002 (2003).
[11] K. T. Chung, T. K. Fang, and Y. K. Ho, J. Phys. B **34**, 165 (2001).
[12] X. M. Tong and C. D. Lin, Phys. Rev. Lett. **92**, 223003 (2004).
[13] I. A. Ivanov and Y. K. Ho, Phys. Rev. A **68**, 033410 (2003).
[14] J. R. Harries and Y. Azuma, Rev. Sci. Instrum. **75**, 4406 (2004).
[15] K. C. Prince *et al.*, Phys. Rev. Lett. **96**, 093001 (2006).
[16] M. Žitnik *et al.*, Phys. Rev. A **74**, 051404(R) (2006).
[17] C. Såthe *et al.*, Phys. Rev. Lett. **96**, 043002 (2006).
[18] M. Žitnik and A. Mihelič, J. Phys. B **39**, L167 (2006).
[19] Y. K. Ho, Phys. Rep. **99**, 1 (1983).
[20] A. Buchleitner, B. Grémaud, and D. Delande, J. Phys. B **27**, 2663 (1994).
[21] G. Lagmago Kamta, B. Piraux, and A. Scrinzi, Phys. Rev. A **63**, 040502(R) (2001).
[22] A. Mihelič, Ph.D. thesis, Faculty of Mathematics and Physics, University of Ljubljana, 2006, http://www.rcp.ijs.si/amihelic/phd/thesis.pdf.
[23] F. Robicheaux *et al.*, Phys. Rev. A **52**, 1319 (1995).
[24] U. Fano, Phys. Rev. **124**, 1866 (1961).
[25] L. Lipsky and M. J. Conneely, Phys. Rev. A **14**, 2193 (1976).
[26] M. Žitnik *et al.*, Phys. Rev. A **65**, 032520 (2002).